



# Dehydration of D-xylose to furfural using different supported niobia catalysts



C. García-Sancho<sup>a</sup>, I. Agirrezabal-Telleria<sup>b,\*</sup>, M.B. Güemez<sup>b</sup>, P. Maireles-Torres<sup>a</sup>

<sup>a</sup> Departamento de Química Inorgánica, Cristalografía y Mineralogía (Unidad Asociada al ICP-CSIC), Facultad de Ciencias, Universidad de Málaga, Campus de Teatinos, 29071 Málaga, Spain

<sup>b</sup> Department of Chemical and Environmental Engineering, Engineering School of the University of the Basque Country (EHU/UPV), Alameda Urquijo s/n, 48013 Bilbao, Spain

## ARTICLE INFO

### Article history:

Received 19 November 2013

Received in revised form 8 January 2014

Accepted 9 January 2014

Available online 19 January 2014

### Keywords:

Xylose dehydration

Furfural

Mesoporous support

Heterogeneous catalysis

Niobium oxide

## ABSTRACT

Solid acids catalysts based on niobium oxide incorporated on different supports (commercial fumed silica and  $\gamma$ -Al<sub>2</sub>O<sub>3</sub>, MCM-41 and SBA-15 silicas) have been synthesized, characterized by using XRD, N<sub>2</sub> sorption at  $-196^\circ\text{C}$ , XPS, Raman spectroscopy, NH<sub>3</sub>-TPD and pyridine adsorption coupled to FTIR spectroscopy, and tested for the dehydration of D-xylose to furfural. A monophasic water and biphasic water/toluene systems were compared, obtaining similar xylose dehydration activity but improving considerably the furfural selectivity when the toluene was employed as co-solvent. The  $\gamma$ -Al<sub>2</sub>O<sub>3</sub> support enhanced apparently the secondary reactions, as can be inferred for the lower furfural selectivity of the Al-12Nb catalyst compared with the silica supported catalysts. The highest conversion and furfural selectivity after 24 h (84% and 93%, respectively) were found for the SBA-12Nb catalyst, at  $160^\circ\text{C}$  in water/toluene. The niobia loading barely affected the xylose dehydration activity, but the catalyst with a 12 wt% showed higher furfural selectivity. Alternative N<sub>2</sub>-stripping technique was also studied, improving the furfural yield and product purity in the stripped stream.

© 2014 Elsevier B.V. All rights reserved.

## 1. Introduction

In recent years, the search and development of alternative sources of fuel and chemicals have gained worldwide attraction because of the depletion of fossil resources, increasing prices, as well as the environmental concerns related to global warming and pollution [1–3]. About 200 billion tons of biomass are produced annually, but less than 3% are used as feedstock for the synthesis of biochemicals or biofuels, thus becoming as an interesting alternative to fossil resources [4]. The major component of plant-derived biomass are carbohydrates, being of great importance to develop efficient and green approaches to their valorization by conversion into high added-value products [5].

Nowadays, furfural is regarded as one of the most outstanding building blocks because of its large spectrum of industrial applications, and its versatility as platform compound for the synthesis of a broad range of chemicals (furfuryl alcohol, 2-methylfuran, tetrahydrofuran, 2-methyltetrahydrofuran, linear alkanes, furoic acid, maleic acid,...) [2]. Furfural is usually obtained from the dehydration of xylose, which is obtained by acid hydrolysis of pentosans coming from hemicellulose (polysaccharides). Currently,

furfural production is based in the traditional batch process of Quaker Oats, employing water as stripping agent and homogeneous acid-catalysts, mainly concentrated sulfuric acid [6]. Nevertheless, mineral acids are highly toxic, corrosive, and difficult to handle and recover, which together with several environmental issues, have driven research efforts to the search of greener solid acid catalysts, stable in water in order to perform this reaction in aqueous solution. In this context, many different heterogeneous catalysts have been reported for the xylose dehydration: zeolites [7–11], bulk and mesostructured sulfated zirconia with or without aluminium incorporation [12,13], porous silicoaluminophosphates [14], exfoliated titanate, niobate and titanoniobate nanosheets [15], bulk or supported heteropolyacids [16,17], sulfonic acid modified mesoporous silica [18–21], exchange resins [22–24], metal oxides [25] and hydroxylated MgF<sub>2</sub> [26].

Niobium containing catalysts have also demonstrated to be active in the dehydration of different saccharides [27–29], due to their excellent acid properties and hydrothermal stability [30]. In order to enhance the dispersion of niobium oxide and increase the number of available active sites, niobium pentoxide has been supported on different high surface area solids, being silica and alumina the most studied [31–34]. Different surface species were produced according to the physicochemical properties of support and the niobium content, showing a straightforward correlation with product selectivity. In this sense, Dias et al. [35] tested crystalline

\* Corresponding author. Tel.: +34 617912295; fax: +34 94 601 4179.

E-mail address: [iker.aguirrezabal@ehu.es](mailto:iker.aguirrezabal@ehu.es) (I. Agirrezabal-Telleria).

### Nomenclature

$[X]_0$	Initial xylose loading (%)
$[X]_R$	Xylose concentration in the reactor ( $\text{g L}^{-1}$ )
$X_X$	Xylose conversion (%)
$[FUR]_0$	Initial FUR loading in the reactor ( $\text{g L}^{-1}$ )
$[FUR]_R$	FUR concentration in the water-phase in the reactor ( $\text{g L}^{-1}$ )
$[FUR]_T$	FUR concentration in the toluene phase ( $\text{g L}^{-1}$ )
$R_I$	Ratio of $[FUR]_T:[FUR]_R$ in biphasic systems
$[FUR]_C$	FUR concentration in the condensate for nitrogen-stripping ( $\text{g L}^{-1}$ )
$FUR_S$	FUR selectivity (%)
$K_S$	Stripping constant for liquid–vapour mass transfer ( $\text{L min}^{-1}$ )
$V_R$	Liquid volume in the reactor (L)
$V_C$	Total volume of stripped condensate (L)
$k$	Kinetic constants in the absence of catalysts
$k'$	Kinetic constants with respect to catalyst mass load

microporous and mesoporous niobium silicates (denoted as AM-11 and Nb-MCM-41, respectively) for dehydration of xylose in batch, using a water–toluene mixture as solvent at 160 °C. Nb-MCM-41 was more active for xylose conversion than microporous AM-11, attaining xylose conversion between 92% and 99% after 6 h, although furfural selectivity was slightly higher for AM-11. Nevertheless, the reusability studies of Nb-MCM-41 catalysts demonstrated that xylose conversion decreased after several recycling runs due to the loss of structural ordering and leaching of niobium species (between 6% and 50% of the initial Nb content). As niobium usually adopts a higher coordination number than silicon, it becomes very difficult to stabilize Nb species into the siliceous framework; however, the impregnation method reported by García-Sancho et al. [36] allowed to reach conversion of 96.8% and a furfural yield of 62.1% over MCM-Nb16 catalyst, at 170 °C after 2 h, in the presence of 0.25 g of NaCl per g of aqueous solution, showing a high stability during three catalytic runs without any intermediate regeneration step. Moreover, the leaching of Nb from MCM-Nb16 represented only 0.05 wt% of the Nb initially present in this solid, and soluble niobium species were inactive in the dehydration of xylose to furfural.

On the other hand, another key aspect to be study in depth during xylose dehydration is related to the furfural yield loss in water, attributed to secondary reactions of furfural with intermediates of the pentose to furfural process (furfural condensations) and furfural with itself (furfural resinification) [6]. Different strategies have been proposed to minimize these undesired side reactions. Hence, as most studies operate in aqueous phase, furfural is simultaneously extracted by using an organic solvent. Notwithstanding toluene has been the most employed co-solvent [7,15–18,37], other organic phases have been also tested to improve furfural yields, such as methylisobutylketone [7,38,39], *n*-butanol [40], dichloromethane [41] and cyclopentyl methyl ether [42]. Nevertheless, the presence of a biphasic system requires additional solvent/furfural separation stages. Alternatively, the use of supercritical fluids has been studied for fast separation processes. Thus, the influence of the furfural extraction by supercritical CO<sub>2</sub> on the furfural yield has been evaluated [43–45]. On the other hand, the use of N<sub>2</sub> as stripping agent under semi-batch conditions has been recently reported [22,46]. Sustainable future furfural manufacturing systems will require renewable sources but also green processes. In this sense, heterogeneously catalyzed and simultaneous N<sub>2</sub>-stripping processes would considerably reduce the catalyst and steam consumption costs (16:1 at the Quaker process)

and thus achieve similar furfural yields, such as the ones using niobium oxide supported on a commercial catalyst [47]. The use of inert stripping agents presents advantages as the easy furfural separation from the condensed vapour-phase stream and its reusability, which would significantly reduce further distillation stages.

Therefore, it has been considered of great interest to perform a more detailed study of niobia supported catalysts, following the impregnation method proposed by García Sancho et al. [36]. With this aim, several niobia supported on different solids have been prepared and tested in the dehydration of xylose to furfural to evaluate the influence of support. In order to develop the industrial application of these catalysts, the dehydration of xylose has been carried out in a larger scale and a longer time to verify their stability. Also, the use of a biphasic liquid system formed by water and toluene, under batch conditions, and nitrogen as stripping agent for water–furfural mixtures have been evaluated. This work aims to give new insights into the niobia acid-catalyzed reaction and to establish relationships between the physicochemical properties of catalysts and the furfural selectivity.

## 2. Experimental

### 2.1. Catalyst preparation

Several high surface area solids were used as supports for niobia: two mesoporous silica (MCM-41 [48] and SBA-15 [49]), a commercial fumed silica (powder, 0.007  $\mu\text{m}$ ; Sigma-Aldrich) and a commercial  $\gamma\text{-Al}_2\text{O}_3$  supplied by REPSOL.

The supported Nb<sub>2</sub>O<sub>5</sub> catalysts were prepared following the incipient wetness impregnation method. Thus, aqueous solutions of niobium oxalate in 0.1 M oxalic acid were used to incorporate different amounts of Nb<sub>2</sub>O<sub>5</sub> on the support (4, 12 and 20 wt%). After impregnation, the materials were dried in air at 60 °C and calcined at 550 °C during 6 h. These materials were denoted as X-*n*Nb, where X indicates the support (MCM, SBA, Si and Al) and *n* represents the weight percentage of Nb<sub>2</sub>O<sub>5</sub> in each catalyst.

### 2.2. Catalyst characterization

Powder XRD patterns were obtained using a Siemens D5000 automated diffractometer, over a  $2\theta$  range with Bragg–Brentano geometry using the Cu K $\alpha$  radiation and a graphite monochromator.

N<sub>2</sub> adsorption–desorption isotherms at –196 °C were obtained using an ASAP 2020 model of gas adsorption analyzer from Micromeritics, Inc. Prior to N<sub>2</sub> adsorption, the samples were evacuated at 200 °C (heating rate 10 °C min<sup>–1</sup>) for 24 h. Pore size distributions and pore volume were calculated with the BJH method.

Raman spectra were recorded on a Raman Senterra (Bruker) micro-spectrometer equipped with a thermoelectrically cooled CCD detector. An Nd:YAG laser was used as the excitation source at 532 nm and the laser power was set to 2 mW. Raman spectra were performed from powder samples without any previous treatment.

X-ray photoelectron spectroscopy (XPS) studies were performed with a Physical Electronics PHI 5700 spectrometer equipped with a hemispherical electron analyzer (model 80-365B) and a Mg K $\alpha$  (1253.6 eV) X-ray source. Charge referencing was done against adventitious carbon (C 1s at 284.8 eV).

Temperature-programmed desorption of ammonia (NH<sub>3</sub>-TPD) was carried out to evaluate the total acidity of the catalysts. After cleaning the materials with helium and adsorption of ammonia at 100 °C, the NH<sub>3</sub>-TPD was performed between 100 and 550 °C with a heating rate of 10 °C min<sup>–1</sup>, by using a helium flow, and maintained at 550 °C for 15 min. The evolved ammonia was analyzed using a TCD detector of a gas chromatograph (Shimadzu GC-14A).

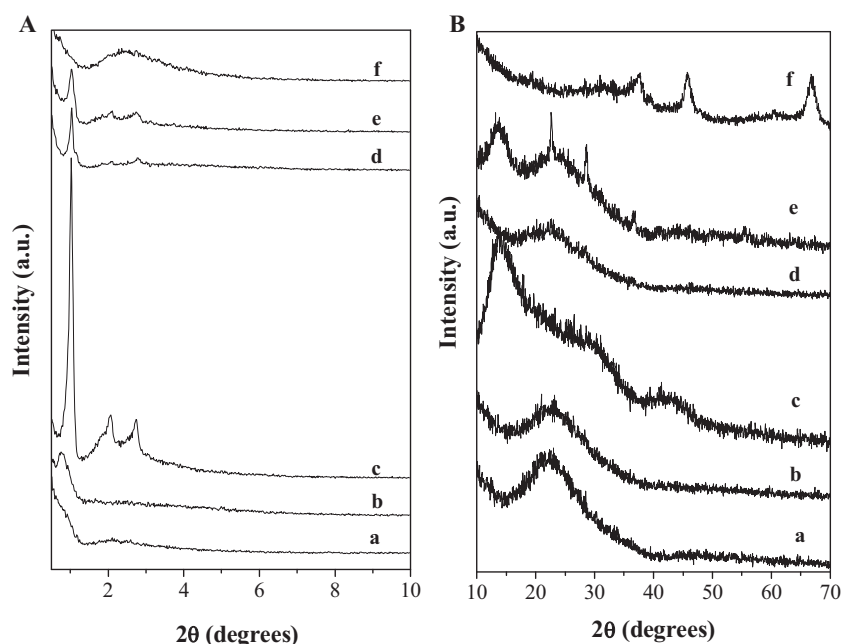


Fig. 1. XRD patterns of *X*-*n*Nb materials at low (A) and at high (B) angle region: (a) Si-12Nb, (b) MCM-12Nb, (c) SBA-4Nb, (d) SBA-12Nb, (e) SBA-20Nb and (f) Al-12Nb.

FTIR spectra of adsorbed pyridine were recorded on a Shimadzu Fourier Transform Infrared Instrument (FTIR8300). Self supported wafers of the samples with a weight/surface ratio of about  $15 \text{ mg cm}^{-2}$  were placed in a vacuum cell greaseless stop-cocks and  $\text{CaF}_2$  windows. The samples were evacuated at  $300^\circ\text{C}$  and  $10^{-2} \text{ Pa}$  overnight, exposed to pyridine vapours at room temperature (vapour pressure of  $200 \text{ mbar}$ ) for 10 min and then outgassed at  $200^\circ\text{C}$ .

Thermogravimetric analyses (TGA) were carried out in a TGA/SDTA 851e module (Mettler–Toledo), measuring the weight variation during oxidation at a heating ramp of  $10^\circ\text{C min}^{-1}$  from room temperature until  $800^\circ\text{C}$ .

### 2.3. Catalytic tests

Xylose dehydration catalytic tests were performed in batch at  $160^\circ\text{C}$ , by using a temperature-controlled stainless-steel reactor (Autoclave Engineers), with controlled electric heating and stirred at 500 rpm. In order to keep the reaction medium in liquid-phase (200 mL of total reaction solution), the system was pressurized at 15 bar. The water/toluene tests were performed with 1:1 v/v water/toluene ratio (water/toluene molar ratio of 5.9). The corresponding xylose solution was initially added to obtain an initial xylose loading of  $20 \text{ g L}^{-1}$ . Catalyst loading was fixed at 20 wt% with respect to initial xylose load and reaction time was set at 24 h. In order to study the catalyst stability, solid catalysts were only recovered by filtration, washed thoroughly with water to remove impurities and dried at room temperature.

The  $\text{N}_2$ -stripping tests were carried out in a 2 L reactor (Autoclave Engineers), with controlled electric heating and stirred at 500 rpm. In a typical SC experiment operating at  $180^\circ\text{C}$  and 10 bar, the reactor was first loaded with the corresponding amount of catalyst and heated up to  $190^\circ\text{C}$  with deionized water (75% of total initial reactor volume). The rest, 25% of total reactor volume, was fed from a nitrogen-pressurized vessel (to reach the corresponding initial xylose concentration,  $X_0$ ). This set-up allowed the xylose solution to be held at room temperature until the desired temperature was reached in the reactor and minimized the initial xylose degradation. During the  $\text{N}_2$ -stripping tests, mass-flow controlled nitrogen was bubbled into the liquid bottom at  $150 \text{ mL min}^{-1}$  (STP)

at room temperature. This gas flow stripped the water-furfural vapour stream. The gaseous flow was later fed to a condenser (cooled by Peltier effect at  $10^\circ\text{C}$ ), where gas and liquid streams were separated. The condensate was continuously weighted. Automatic control valves were used to regulate the reactor-pressure and liquid level in the condenser.

Xylose and furfural were quantified in a 1260 Infinity module from Agilent. The products, after dilution in water, were separated in a Zorbax SB-C18 column ( $3.5 \mu\text{m}$ ,  $3.0 \times 150 \text{ mm}$ ) at  $1 \text{ mL min}^{-1}$  and  $35^\circ\text{C}$  using water as eluent. Secondary products were identified by GC–MS (6890 GC and 5973-Mass Selective Detector from Agilent) using a DB-FFAP column, helium as carrier gas at  $1 \text{ mL min}^{-1}$  and an injection volume of  $1 \mu\text{L}$ .

The xylose conversion ( $X_X$ ) and FUR selectivity ( $\text{FUR}_S$ ) were calculated as follows:

$$X_X = 1 - \frac{\text{mol of xylose in the reactor}}{\text{initial mol of xylose}}$$

$$\text{FUR}_S = \frac{\text{mol of furfural in the reactor}}{\text{mol of converted xylose}}$$

## 3. Results and discussion

### 3.1. Characterization of materials

In order to check the support stability after the impregnation with niobium oxalate and subsequent calcination at  $550^\circ\text{C}$ , catalysts were characterized by X-ray diffraction. The powder X-ray diffraction patterns (Fig. 1A) of MCM-12Nb and SBA-*n*Nb in the  $2\theta$  range of  $0.5$ – $10^\circ$  confirmed that the long-range order of the mesostructured support was maintained after niobium incorporation. Thus, a broad and intense diffraction peak was observed for MCM-12Nb, which could be assigned to the (100) diffraction signal of the mesoporous MCM-41 silica support. On the other hand, the low-angle powder XRD patterns of the SBA-*n*Nb catalysts also exhibited a very intense peak at  $ca. 2\theta = 1.05^\circ$  corresponding to (100) reflection, together with other three weaker peaks between  $2$  and  $3^\circ$ , associated to the (110), (200) and (210) planes in a hexagonal arrangement. These results are consistent with those previously reported by Gómez-Cazalilla et al. [49]. Nevertheless, an attenuation of the diffraction peak as the niobium loading increased

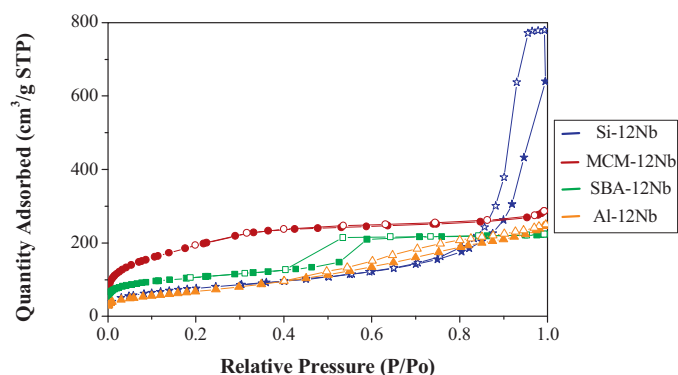


**Fig. 2.** Nitrogen adsorption (solid symbol)–desorption (open symbol) isotherms of X-12Nb.

(SBA-12Nb and SBA-20Nb) was detected, which could be explained by the partial disorder of the silica framework during calcination step, because of the exothermic decomposition of the large amount of oxalate precursor used for preparing these catalysts, as observed by Li et al. [50]. Regarding the XRD patterns in the high-angle region, the characteristic reflections of crystalline  $\text{Nb}_2\text{O}_5$  phases were not found, pointing to the presence of either amorphous particles or small sized Nb species on the silica surface (Fig. 1B). Only for the highest niobia loading, SBA-20Nb, XRD peaks assigned to hexagonal  $\text{Nb}_2\text{O}_5$  phases were observed. Likewise, the presence of crystalline  $\gamma\text{-Al}_2\text{O}_3$  was detected for Al-12Nb in its high-angle XRD pattern.

Textural properties of catalysts were evaluated by nitrogen adsorption–desorption isotherms at  $-196^\circ\text{C}$ . All the niobium-containing catalysts exhibited Type IV isotherms according to the IUPAC classification (Fig. 2), as well as average pore sizes centered in the mesoporous range, thus confirming that all materials retain their mesoporous character after impregnation with  $\text{Nb}_2\text{O}_5$ . The shape of the isotherms was also preserved for different amounts of niobia over SBA-15 (not shown). However, the BET surface areas and pore volumes (Table 1) generally decreased when niobium oxide was incorporated to the support. Besides, this reduction was higher for increasing Nb loading, mainly above 12 wt% over SBA-15; this may be due to the exothermic decomposition of the higher amounts of oxalate precursor which could partially destroy the

**Table 1**  
Textural data of the catalysts.

Catalyst	$S_{\text{BET}}$ ( $\text{m}^2 \text{g}^{-1}$ )	Pore volume ( $\text{cm}^3 \text{g}^{-1}$ )	Av. pore diameter (nm)
$\text{SiO}_2$	425	0.946	10.7
Si-12Nb	278	1.205	17.4
MCM-41	1441	1.165	2.9
MCM-12Nb	691	0.434	3.1
SBA-15	604	0.518	3.7
SBA-4Nb	576	0.478	3.5
SBA-12Nb	351	0.344	3.7
SBA-20Nb	365	0.344	3.7
$\text{Al}_2\text{O}_3$	279	0.414	6.4
Al-12Nb	252	0.387	6.0

long-range order, as previously indicated. On the other hand, the average pore diameters barely changed, thus corroborating that  $\text{Nb}_2\text{O}_5$  particles are homogeneously dispersed on the surface of the support and do not block their mesopores.

In order to get insights into the surface nature of catalysts, X-ray photoelectron spectroscopy was used for their characterization. The XPS data are summarized in Table 2. The binding energy (BE) values observed for Si 2p in supported catalysts over different silica were between 103.4 and 103.6 eV, in agreement with the data of Si in silica. In the same way, the BE value of Al 2p for the Al-12Nb catalyst (74.4 eV) was typical of  $\gamma\text{-Al}_2\text{O}_3$ . The O 1s region only showed an almost symmetric peak at 531.11 eV for Al-12Nb and between 532.7 and 532.9 eV for silica catalysts (Fig. 3A), which corresponded with the oxygen signal in  $\gamma\text{-Al}_2\text{O}_3$  and  $\text{SiO}_2$ , respectively, confirming the absence of segregated niobia particles on the external surface of the support. However, a broadening of the O 1s signal was found for SBA-20Nb, which may be due to the presence of segregated  $\text{Nb}_2\text{O}_5$  particles or even other niobium oxide species on the external surface of SBA-15, as was inferred from XRD. On the other hand, the binding energy values of the two components of the Nb 3d doublet were in the typical range of Nb(V) in an oxidic environment (Fig. 3B). Nevertheless, broader bands were found for niobium oxide over SBA-15. In fact, the  $3d_{5/2}$  band could be deconvoluted into two components for SBA-20Nb, considering that the resolution improves as the  $\text{Nb}_2\text{O}_5$  content increases, with binding energies of 206.3 and 207.8 eV in agreement with the presence of  $\text{Nb}_2\text{O}_5$  crystallites and well dispersed niobium oxide on the support, respectively. It is unlikely that this lower binding

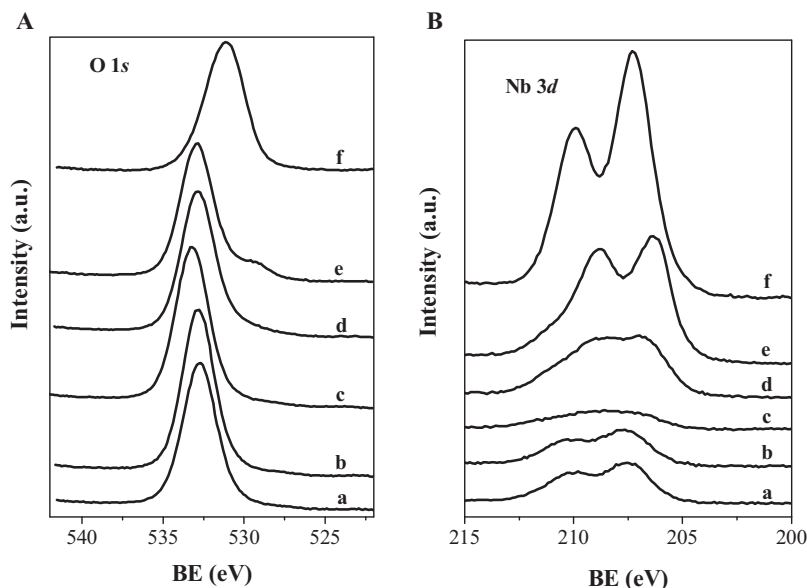


**Fig. 3.** XPS spectra of catalysts in the O 1s (A) and Nb 3d (B) regions: (a) Si-12Nb, (b) MCM-12Nb, (c) SBA-4Nb, (d) SBA-12Nb, (e) SBA-20Nb and (f) Al-12Nb.

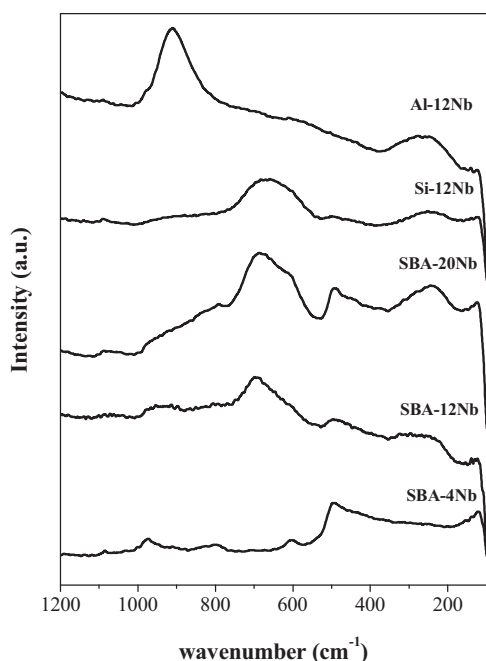


Fig. 4. Raman spectra of catalysts.

energy state belongs to the reduction of  $\text{Nb}_2\text{O}_5$  because Nb,  $\text{NbO}$  and  $\text{NbO}_2$  are expected at 202.2, 203.7 and 205.7 eV, respectively [51]. Likewise, surface Si(Al)/Nb atomic ratio were higher than the theoretical ones, being noteworthy for Si-12Nb and MCM-12Nb. It could be observed that the surface Si/Nb atomic ratio for SBA- $x$ Nb catalysts approached to the postulated ratio when the niobia loading was increased, being very close for SBA-20Nb and corroborating the possible presence of larger crystalline  $\text{Nb}_2\text{O}_5$  particles on the external surface in this catalyst, as was detected by XRD. In the case of Al-12Nb, the surface Al/Nb ratio was lower, so it could exist Nb located on the external surface, although not detected by XRD.

The surface metal oxides are often responsible for the catalytic performance of supported oxides and Raman spectroscopy is a powerful tool to identify the nature of surface metal oxide species. The Raman spectra of niobia catalysts are presented in Fig. 4. No perceptible signal was found for MCM-12Nb, indicating that the niobium oxide species were well dispersed on the surface of MCM-41. A broad band in the 500–750  $\text{cm}^{-1}$  region was found for the rest of silica supported catalysts, although it was almost indiscernible for the SBA-4Nb catalyst. This band may be associated to slightly distorted octahedral  $\text{NbO}_6$  structures which is related to the existence of Brønsted acid sites. However, it was not detected for the Al-12Nb catalyst; in turn, a band in the 800–1000  $\text{cm}^{-1}$  region, which could be attributed to highly distorted octahedral  $\text{NbO}_6$

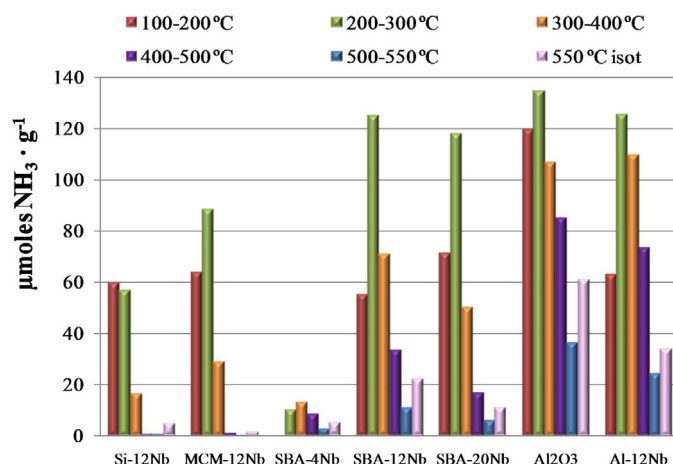


Fig. 5.  $\text{NH}_3$ -TPD measurements performed for different catalysts as a function of desorption temperature.

structures associated to the Lewis acid sites, was present. This band was barely observed for SBA-4Nb and SBA-12Nb. Additional Raman bands between 200 and 300  $\text{cm}^{-1}$  demonstrated that crystalline  $\text{Nb}_2\text{O}_5$  nanoparticles were present in SBA-20Nb, and Al-12Nb. In addition, it could be observed for the SBA-12Nb catalyst, but it was not found for SBA-4Nb. Thus, the intensity of the Raman bands in this region also increased with the  $\text{Nb}_2\text{O}_5$  loading, as reported by Jehng et al. [31]. Finally, a band at 492  $\text{cm}^{-1}$  was found for SBA-15 materials which could be assigned to tetra-cyclosiloxane rings [52].

It is well known that activity in the xylose dehydration into furfural depends on the strength of acid sites, so the total acidity was evaluated by  $\text{NH}_3$ -TPD. Firstly, the acidity of different supports was measured, being almost zero for silica supports; however,  $\gamma$ - $\text{Al}_2\text{O}_3$  showed an acidity of 543.5  $\mu\text{mol NH}_3 \text{ g}_{\text{cat}}^{-1}$ . In general, the total acidity of catalysts (Table 3) largely increased with respect to the pristine support, except for Al-12Nb. Likewise, the total acidity increased when the Nb content risen from 4 to 12 wt%, corroborating the suitable dispersion of the active  $\text{Nb}_2\text{O}_5$  phase. However, the acidity of SBA-20Nb was lower than that of SBA-12Nb, which may be due to the formation of large niobia clusters for the highest Nb content. Table 3 also exhibits the acidity values, expressed as  $\mu\text{moles of NH}_3$  per surface unit, reaching the highest acid sites density for Al-12Nb and SBA-12Nb. On the other hand, the  $\text{NH}_3$ -TPD profiles (not shown) revealed the presence of acid centers with a broad range of strength. In addition, it is generally accepted that the acid strength depends on the ammonia desorption temperature [53], being ammonia desorbed from stronger sites at higher temperatures. Therefore, the number of acid sites of different strength was calculated integrating in different temperature ranges (Fig. 5), resulting that, in all cases, most of

Table 2  
XPS data for fresh and spent (R) catalysts.

Catalyst	Binding energy (eV)			Atomic concentration (%)					
	O 1s	Si (Al) 2p	Nb 3d <sub>5/2</sub>	C	O	Si (Al)	Nb	Si (Al)/Nb <sub>XPS</sub>	Si (Al)/Nb <sub>theor</sub>
Si-12Nb	532.7	103.4	207.5	2.47	64.57	32.04	0.92	34.82	16.24
RSi-12Nb	532.6	103.4	207.3	42.29	41.90	15.45	0.36	42.91	
MCM-12Nb	532.8	103.4	207.6	6.26	62.69	30.27	0.77	39.31	16.24
RMCM-12Nb	532.7	103.4	207.2	30.64	48.89	19.57	0.91	21.51	
SBA-4Nb	532.8	103.4	Very broad	3.06	64.08	32.37	0.49	66.06	53.16
SBA-12Nb	532.8	103.5	Very broad	3.76	63.07	31.49	1.69	18.63	16.24
RSBA-12Nb	532.8	103.4	207.5	36.01	45.58	17.79	0.61	29.16	
SBA-20Nb	532.9	103.6	206.3	4.45	64.50	28.12	2.92	9.63	8.86
	529.8		207.8						
Al-12Nb	531.1	74.43	207.2	3.82	60.48	31.45	4.25	7.4	19.12
RAI-12Nb	531.8	531.8	207.4	71.05	25.09	3.51	0.34	10.32	

**Table 3**  
Acidic properties of supported niobia catalysts and catalytic activity for xylose dehydration in water/toluene at 160 °C.

Catalyst	Acidity ( $\mu\text{mol NH}_3 \text{ g}_{\text{cat}}^{-1}$ )	Acid-density ( $\mu\text{mol NH}_3 \text{ m}^{-2}$ )	$C_L/(C_B + C_L)^a$	$X_R^b$ (%)	$\text{FUR}_R^b$ (%)	$\text{TOF} \times 10^2$ ( $\text{mmolX}(\mu\text{mol h})^{-1}$ ) <sup>c</sup>	$k_1 \times 10^3$ ( $\text{min}^{-1} \text{ g}_{\text{cat}}^{-1}$ )	$k_2 \cdot 10^3$ ( $\text{L min}^{-1} \text{ g}_{\text{cat}}^{-1}$ )	$C^d$ (%)
Al-12Nb	430.4	1.71	0.73	62 (75)	59 (61)	0.80	7.3	1.8	15.45
Si-12Nb	139.2	0.50	0.61	42 (82)	80 (80)	1.66	5.1	0.6	12.91
MCM-12Nb	183.9	0.27	0.68	35 (80)	88 (84)	1.06	4.2	0.5	8.89
SBA12-Nb	318.1	0.91	0.90	38 (85)	92 (93)	0.66	3.9	0.5	13.42
TSBA12-Nb				84 <sup>e</sup>	60 <sup>e</sup>				
SBA-4Nb	39.9	0.07	0.68	81 <sup>f</sup>	92 <sup>f</sup>				
SBA-20Nb	273.2	0.75	0.41	40 (91)	71 (61)	5.51			
				35 (86)	67 (73)	1.21			

<sup>a</sup> Concentration of acid sites calculated from the extinction coefficients calculated by Datka et al. [32].

<sup>b</sup> Xylose conversion ( $X_R$ ) and FUR selectivity ( $\text{FUR}_R$ ) measured at 4 h and 24 h (in brackets).

<sup>c</sup> Turnover frequency based on converted xylose at 4 h and catalyst initial acidity in  $\mu\text{mol/g}$ .

<sup>d</sup> Xylose conversion and furfural selectivity values obtained after 3 h of reaction using simultaneous  $\text{N}_2$ -stripping at 180 °C.

<sup>e</sup> %C by CHN analysis of used catalysts.

<sup>f</sup> Activity data of used and regenerated SBA12-Nb (at 500 °C) after 24 h at 160 °C in water/toluene.

ammonia molecules were desorbed between 100 and 400 °C. Nevertheless, an appreciable contribution to the total acidity was found between 400 and 550 °C for the supported catalysts over SBA-15 and mainly for Al-12Nb, evidencing the heterogeneous distribution of acid sites and the presence of strong acid sites in these catalysts. In the case of Al-12Nb, this strong acidity had already been observed in the pristine support, so it would not correspond to the acidic niobium oxide sites. However, it did not appear for the SBA-15 support, so it could be generated from the stronger niobia-silica interaction.

In order to evaluate the amount and type of acidic sites, pyridine adsorption coupled to FTIR spectroscopy was employed. It is known that peaks at  $1450 \text{ cm}^{-1}$  (19b vibration) and  $1610\text{--}1620 \text{ cm}^{-1}$  (8a vibration) are characteristic of pyridine coordinated Lewis acid sites, being the intensity of the 19b band proportional to the total number of Lewis sites and the 8a band related to the strength of these sites [54]. Pyridine interacts also with Brönsted acid sites, giving rise to a band near  $1550 \text{ cm}^{-1}$ . Thus, the concentration of both types of acid sites was estimated from the integrated areas of the bands at  $1550$  and  $1450 \text{ cm}^{-1}$ , using the extinction coefficients  $E_B = 0.73 \text{ cm} \mu\text{mol}^{-1}$  and  $E_L = 1.11 \text{ cm} \mu\text{mol}^{-1}$  for Brönsted and Lewis sites, respectively [32]. Both types of sites were found for all catalysts, being generally higher the concentration of Lewis sites. The total acidity was lower than that obtained by  $\text{NH}_3$ -TPD because the ammonia size is smaller, thus allowing its easy access to most of acid sites, being also different the adsorption temperature. It is known that incorporation of niobia to silica creates Lewis and Brönsted acid sites, which were not found for silica itself. However, when it was incorporated to the alumina support, new Brönsted and Lewis acid sites were generated whereas some Lewis Al sites, associated to the alumina support, disappeared [32]. The amount of Lewis acid sites increased as the Nb content rose from 4% to 12%, but decreased for SBA-20Nb (Table 3), as was detected by  $\text{NH}_3$ -TPD. The highest  $C_L/(C_B + C_L)$  ratio were found for SBA-12Nb and Al-12Nb, which also exhibited characteristic Lewis acid signals in the corresponding Raman spectra. The 8a vibration (not shown) only was preserved after outgassing at 200 °C for the Al-12Nb catalyst, thus pointing the existence of strong Lewis acid sites.

### 3.2. Activity of xylose dehydration to furfural

#### 3.2.1. Catalyst screening under batch conditions

Acid catalysts containing Lewis sites, like hydrated niobia, were recently reported as hydrothermally stable [30]. The hydroxylation of the Lewis acid sites had little effect on the corresponding catalytic activity. On the other hand, the use different solvents than water, such as the organic Lewis base dimethylsulfoxide (DMSO), might reduce the Lewis acid concentration on the catalyst surface. For this reason, and aiming to apply the studied materials at an industrial scale, the xylose dehydration to furfural was previously studied under hydrothermal conditions. This study was carried out as a preliminary catalyst screening to evaluate the efficiency of each catalyst under water and water/toluene biphasic conditions.

The addition of toluene to the system barely affected the xylose dehydration activity, although increased significantly the furfural yield due to its extraction efficiency. Xylose conversion and furfural degradation reactions were ruled by the xylose and furfural concentration, as well as by the corresponding kinetic constants (Eqs. (1) and (2), where  $X_R$  and  $\text{FUR}_R$  represent the xylose and furfural concentration in the water-phase, respectively) [46]. The removal of furfural from the reaction medium should reduce the secondary reactions derived from condensation ( $k'_2$ ) and ( $k'_3$ ), mainly occurring in water. However, the xylose dehydration kinetic differences between water and water-toluene systems were not important.

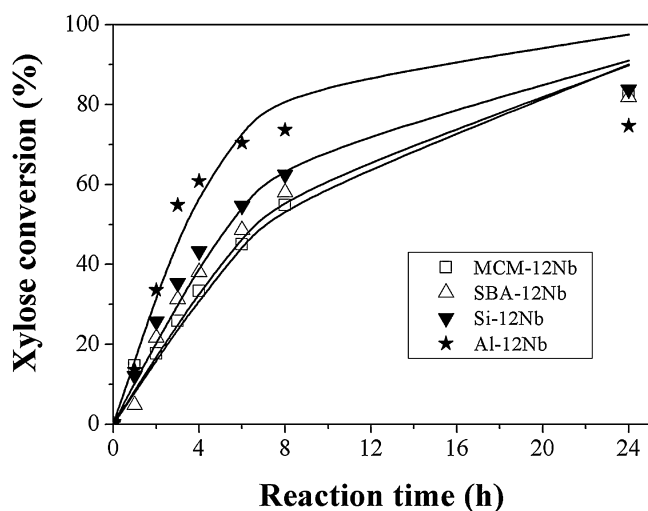


**Fig. 6.** Experimental (bullets) and modelled (continuous line) values of xylose dehydration activity tests carried out in water at 160 °C.  $X_0$ : 2 wt% and catalyst load: 0.3 with respect to  $X_0$ .

These differences were more significant on the furfural degradation reactions occurring in the monophasic aqueous phase.

$$\frac{dX_R}{dt} = -k'_1 X_R - k'_2 X_R \text{FUR}_R \quad (1)$$

$$\frac{d\text{FUR}_R}{dt} = -k'_1 X_R - k'_2 X_R \text{FUR}_R - k'_3 X_R \text{FUR}_R \quad (2)$$

Fig. 6 represents the xylose dehydration and Fig. 7 shows the corresponding furfural selectivities on the different supported niobia catalysts under water (a) and water-toluene (b) conditions. The kinetic activity and furfural yield are strictly related to the textural properties and nature and density of acid sites. As observed in Table 3, Al-12Nb showed the highest amount and density of acid sites. On the other hand, data derived from the  $N_2$  physisorption analysis of the Si-12Nb sample showed an average pore diameter of 17.4 nm, whereas SBA-12Nb and MCM-12Nb catalysts exhibited intermediate acidities and pore sizes in the lower mesopore range ( $\sim 3$  nm). According to the kinetic data, the Al-12Nb catalyst displayed the highest initial conversion rate, but with a TOF value lower than the Si-12Nb sample. In this sense, the different accessibility to the acid sites located into the porous network could give rise to significant differences in catalytic performances. Thus, the Si-12Nb catalyst presented a larger pore size, favouring the diffusivity of xylose and consequently the dehydration activity. Regardless of a  $C_L/(C_L + C_B)$  ratio lower than the rest of samples with a similar loading (12 wt%), the diffusion effects in Si-12Nb predominated over its acidity. However, although the Al-12Nb catalyst already contained Lewis and Brønsted sites on the fresh support, materials such as  $\gamma\text{-Al}_2\text{O}_3$ , presenting higher Lewis acidity than Brønsted, showed the highest xylose dehydration activity but poor furfural selectivity, as reported in the literature [55]. The grafting of extra acid sites increased the strength of the surface acidity (as shown in Fig. 5), showing an increment of the xylose dehydration activity in the first 8 h of reaction, but lower TOF values (based on xylose conversion per acid site). The MCM-12Nb and SBA-12Nb catalysts, given their similar textural properties and intermediate acidity, exhibited similar dehydration activities. In summary, it could be concluded that the key parameters determining xylose dehydration activity were the total acid site content and the textural properties of supports. Recent studies reported the influence of the Lewis/Brønsted ratio on the catalytic performance [26,55]. Based on catalysts with similar textural properties and

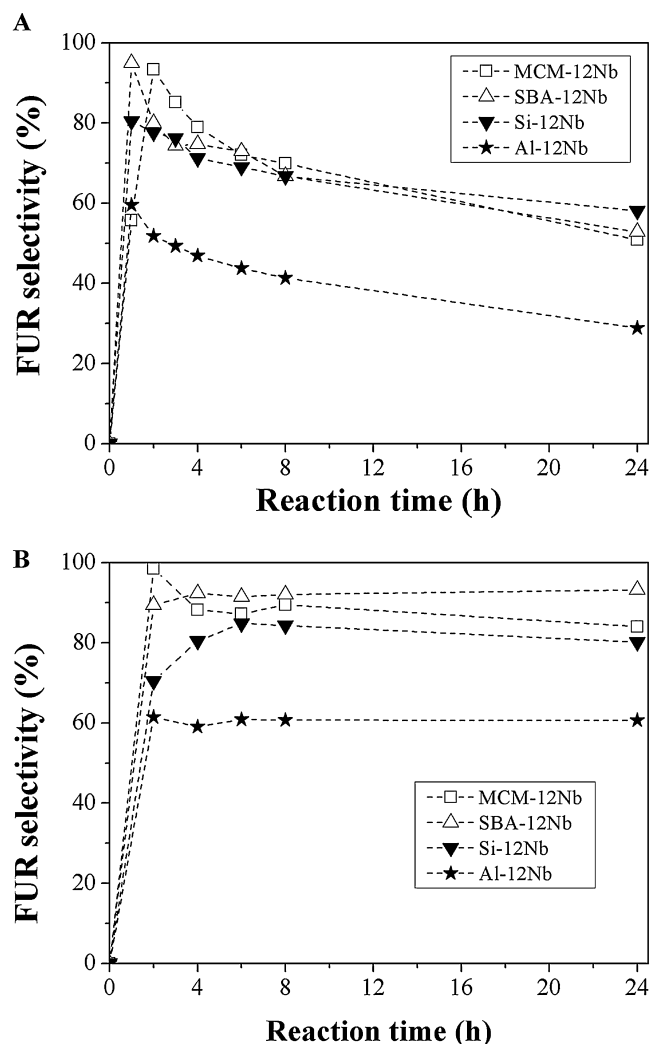


**Fig. 7.** Experimental values of the furfural selectivity on the xylose dehydration tests carried out in water (A) or in water/toluene (B) at 160 °C.  $X_0$ : 2 wt% and catalyst load: 0.3 with respect to  $X_0$ .

acid-site densities, the Lewis acid-sites promoted a faster xylose dehydration rate to yield a xylulose isomer, which required Brønsted sites to be further dehydrated to furfural. On the other hand, materials featuring high Brønsted site densities showed lower dehydration rates but higher furfural selectivity [26]. However, it seems that the contribution of the different acid-sites of the niobia modified catalysts on the catalytic activity was lower than reported, and mainly ruled by the textural properties of the supports and the total acidity.

The experimental data were also modelled (using Eqs. (1) and (2)) based on the gathered kinetic data. The kinetic constants ( $k'_1$  and  $k'_2$ , expressed with respect to catalyst weight) were iterated until reaching the tolerance range specified as least-squares sum (the resinification  $k'_3$  value was directly obtained from FUR+catalyst tests in water and showed an average value of  $1.25 \times 10^{-3} \text{ min}^{-1} \text{ g}_{\text{cat}}^{-1}$ ). As observed in Table 3, the correlation between the dehydration activities displayed in Fig. 6 and the  $k'_1$  values was good in the first 8 h of reaction (higher activities imply higher  $k'_1$  values). However, as observed in Fig. 6, the modelled lines after 8 h tended to shift from the experimental values. This behaviour could be mainly attributed to deactivation effects of active acid-sites. The presence of humin deposits on the used niobia modified catalysts (as evidenced by TGA) provoked a decay of the xylose dehydration activity compared

to an ideal non-deactivated acid catalyst. For this reason, the kinetic constant values in Table 3 correspond to the first 8 h of reaction.

The FUR selectivity values during the experiments carried out at 160 °C, in water and water/toluene, are represented in Fig. 7. Toluene acted as an efficient extracting agent to increase the FUR selectivity about 30% compared to monophasic aqueous system. The Al-12Nb catalyst showed a very different selectivity FUR to that of supported silica catalysts. Apparently, the  $\text{Al}_2\text{O}_3$  support enhanced the secondary reactions (especially that associated to secondary reactions,  $k'_2$ , as observed in Table 3). The Al-12Nb sample exhibited a significantly higher acid-site density, which might favour side reactions on the catalyst surface. Indeed, the existence of strong acid-sites, as revealed by the  $\text{NH}_3$ -TPD data, could give rise to higher side reaction rates. Among the modified silica catalysts, the larger pores in the Si-12Nb catalyst could enhance the mobility of furfural through the pores, thus accelerating side reactions. The FUR production displayed by this catalyst is noteworthy, since the FUR selectivity increased in the first 8 h of reaction (Fig. 7B). This behaviour could be explained by considering that the presence of a relatively low amount of Lewis acid sites (low  $C_L/(C_L + C_B)$  ratio) made unfavourable the formation of the xylulose intermediate, which was further converted to FUR; so FUR production was somehow “delayed” compared to samples containing higher  $C_L/(C_L + C_B)$  ratio values. Comparing the SBA-12Nb and MCM-12Nb catalysts, even if SBA-12Nb showed a higher acid site density, its micro-mesoporous structure could provide higher xylose dehydration rates to furfural. FUR selectivities in water decayed after the 2nd hour. However, when toluene was used, FUR could be easily extracted, and a FUR selectivity of 93% was achieved at 85% xylose conversion, at 160 °C and 24 h in water/toluene with the SBA-12Nb sample.

### 3.2.2. Influence of the $\text{Nb}_2\text{O}_5$ loading on SBA catalysts

The results presented in Section 3.1.1 have shown that the highest yield was achieved for catalysts prepared using SBA-15 as support. For this reason, this mesoporous silica support was chosen to evaluate the influence of the niobia loading on the catalytic activity (Fig. 8A). The xylose dehydration activities clearly showed that the different acid site content of catalysts with 4 and 12 wt% barely affected the xylose dehydration activity, which could be attributed to a lower accessibility of the xylose to all the acid sites present in the SBA-12Nb catalyst compared to SBA-4Nb. On the other hand, the SBA-20Nb sample, showing a higher niobium content but lower Lewis/Brønsted ratio, exhibited a similar xylose dehydration activity as the SBA-4Nb, as could be inferred from data of Table 3. This could be explained by the fact that the reduction in the Lewis/Brønsted ratio could be compensated by the total amount of acid-sites, in this case mainly Brønsted sites. According to the FUR production rates (Fig. 8B), the catalyst containing the highest amount of acid site (SBA-12Nb) showed the highest FUR selectivity, whilst that with low Lewis acid sites content (SBA-4Nb) was not able to dehydrate xylose intermediates. On the other hand, higher niobia contents on SBA-20Nb surface selectively produced more furfural than SBA-4Nb, especially due to a lower Lewis/Brønsted ratio.

### 3.2.3. $\text{N}_2$ -stripping

Although toluene is a very efficient extracting agent, as proved in Sections 3.2.1 and 3.2.2, its potential for biomass processes at an industrial scale is limited due to the additional purification stages required. The abundant water present in the raw biomass would require the exclusive use of water as reaction medium, as in the current manufacturing processes. In this sense, alternative separation techniques such as  $\text{N}_2$ -stripping become promising, even

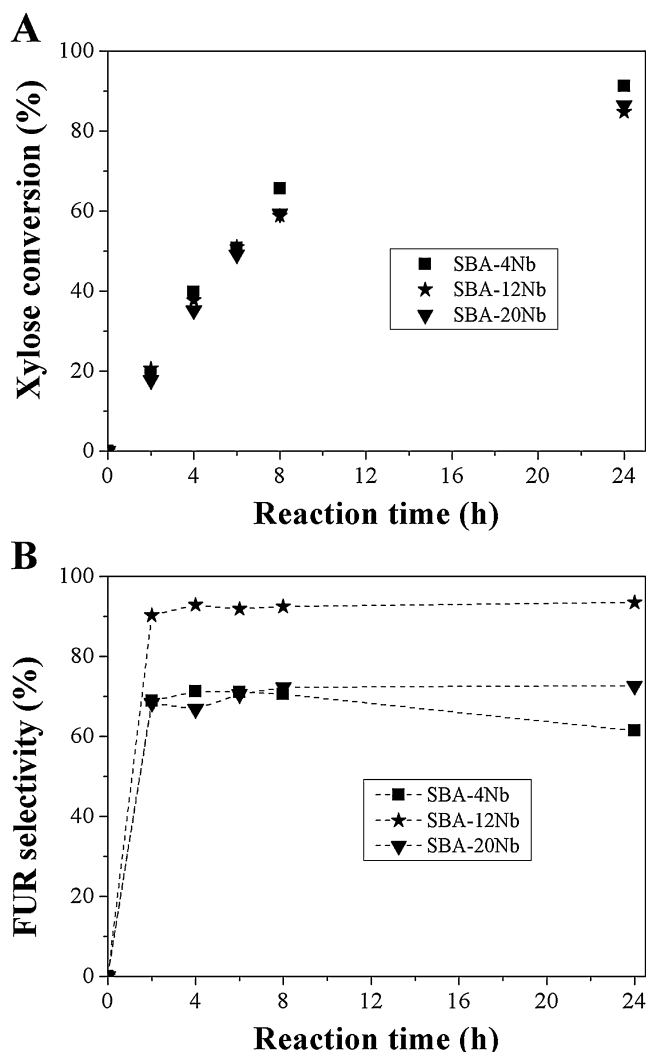


Fig. 8. Experimental values of the xylose dehydration activity (A) and the furfural selectivity (B) for tests carried out in water/toluene at 160 °C for different Nb wt% SBA catalysts.  $X_0$ : 2 wt% and catalyst load: 0.3 with respect to  $X_0$ .

applicable at industrial scale with minimal modifications of the current process.

In this context, the SBA-12Nb catalyst, which displayed the highest furfural yield, was tested at 160 and 180 °C under simultaneous  $\text{N}_2$  stripping. However, catalyst acidity needs to be strong enough to overcome the drawbacks associated to short reaction periods (3 h) and small reaction volumes ( $\sim 7 \text{ mL min}^{-1}$ ), as well as relatively high xylose content. It has been previously demonstrated that xylose dehydration rate at 160 °C is rather low (10%  $X_X$ ) even in the presence of pure Brønsted-type as Amberlyst-70 or  $\text{Nb}_2\text{O}_5$  modified mesoporous catalysts. By using these catalysts, catalyst loadings higher than 60% would be required to achieve reasonable conversion/extracting rate ratios. As observed in Table 3, the catalytic study at 180 °C showed a xylose conversion of 84% and a FUR selectivity of 60%. The stability of heterogeneous  $\text{Nb}_2\text{O}_5$  modified catalysts is crucial to understand the reaction kinetics and evaluate their possible applicability (see Section 3.3). Even if the FUR selectivities were lower than those found with biphasic water/toluene batch systems, it is worth mentioning that the GC-MS analyses of the stripped streams showed a FUR selectivity of nearly 98%. The absence of by-products in the condensate stream would facilitate and reduce further FUR purification stages compared to the current steam-stripping process.

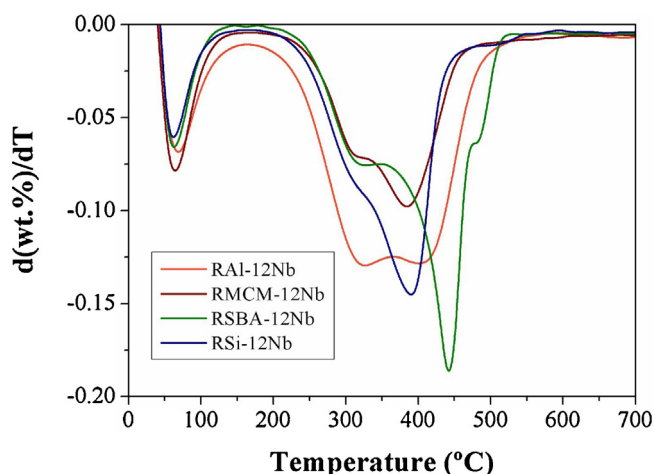


Fig. 9. TGA data of used X-12Nb catalysts.

### 3.3. Humins characterization, the stability and regenerability of catalysts

It is well known that selectivity to FUR in xylose dehydration processes decreases due to the formation of humins, which can be adsorbed on the catalyst surface. In order to characterize adsorbed species, spent catalysts were recovered after each catalytic test by filtration, washed with water and ethanol and dried in air. The amount of carbon deposited on the catalysts was measured by CHN analysis (Table 3), and the found C contents followed the same trend as the acid sites density. Although the Al-12Nb catalyst had shown the highest initial conversion rate, its deactivation was more significant than for the rest of silica modified samples. The highest percentage of carbon (15.45%) and acid sites density were found for this catalyst. The determination of the carbon content in spent catalysts by XPS evidenced much higher values than those obtained by CHN analysis, thus pointing out that carbonaceous species were mainly deposited on the external surface of catalysts (Table 2). Therefore, these adsorbed species are blocking the more accessible acid sites and provoking a reduction of the xylose dehydration activity. Although no significant differences were found between the BE values for the fresh and used catalysts, the surface niobium content was lower on the surface of spent catalysts, as indicated the surface atomic ratios, except for the MCM-12Nb catalyst. This fact revealed that these carbonaceous species were mainly located on niobia particles, which were responsible of the acidity of these catalysts.

The thermal stability of humin deposits was studied by TGA under oxidative conditions (Fig. 9). The thermogravimetric curves displayed two different desorption steps. The first one was probably due to adsorbed water, since it occurred below 100 °C and it was comparable for all catalysts. However, the shape of the second desorption step was different depending if the matrix is silica or alumina, indicating the presence of different types of carbonaceous deposits on the catalysts surface. In all cases, this desorption band was found between 250 °C and 500 °C. For the Al-12Nb catalyst, two bands were clearly visible at 325 °C and 400 °C. However, in the case of modified silica catalysts, a peak at high temperature with a shoulder at lower temperature was observed. In addition, it was observed that the stronger acidic catalysts, SBA-12Nb and Al-12Nb, extended the weight loss until higher temperatures.

Therefore, taking into account these features, the regeneration of spent catalysts was accomplished by thermal treatment at 500 °C under oxygen (named as TSBA12-Nb), thus allowing the calcination of the carbonaceous deposits. The treated catalyst was further reused under the same reaction conditions (160 °C and 20 g L<sup>-1</sup>).

According to the activity data in water/toluene (Table 3), the xylose conversion was slightly reduced from 85% to 81% but the selectivity value was maintained at 92% after 24 h, proving the high stability of the niobia type acid-sites on SBA-15 supported catalysts and the full thermal regeneration of the acid-surfaces. These properties confirm the potential of niobia modified mesoporous supports as suitable heterogeneous acid-catalysts for the conversion of xylose to furfural.

## 4. Conclusions

Different supported niobia catalysts have been demonstrated to be active for the dehydration of xylose to furfural. The use of a co-solvent as toluene improved largely the furfural selectivity (between 20% and 30%), although it hardly affected to the xylose dehydration activity. The deactivation was stronger for the Al-12Nb catalyst, which could be explained by the enhancement of secondary reactions due to the higher acid-site density when  $\gamma$ -Al<sub>2</sub>O<sub>3</sub> was used as support. The micro-mesoporous structure of SBA-12Nb and MCM-12Nb provided higher xylose dehydration rates to furfural than the commercial silica, achieving a xylose conversion of 85% and furfural selectivity of 93% at 160 °C and 24 h in water/toluene with the SBA-12Nb catalyst. Although other niobium oxide contents were studied (SBA-4Nb and SBA-20Nb), the catalyst containing the highest amount of acid sites (SBA-12Nb) displayed the highest furfural selectivity; also, the SBA-12Nb catalyst was reused after regeneration by thermal treatment at 500 °C, demonstrating its high stability. Considering that the use of N<sub>2</sub> stripping has several environmental advantages with respect to co-solvents, the SBA-12Nb catalyst was also tested under simultaneous N<sub>2</sub> stripping, obtaining a furfural purity in the condensate stream of almost 100%.

## Acknowledgements

The authors are grateful to the Spanish Ministry of Economy and Competitiveness (CTQ-2012-38204-C03-02 and CTQ-2012-38204-C03-03), Junta de Andalucía (P09-FQM-5070) and FEDER funds for financial support.

## References

- [1] A.S. Mamman, J.-M. Lee, Y.-C. Kim, I.T. Hwang, N.-J. Park, Y.K. Hwang, J.-S. Chang, J.-S. Hwang, *Biofuels, Bioprod. Biorefin.* 2 (2008) 438–454.
- [2] L. Hu, G. Zhao, W. Hao, X. Tang, Y. Sun, L. Lin, S. Liu, *RSC Adv.* 2 (2012) 11184–11206.
- [3] D.M. Alonso, J.Q. Bond, J.A. Dumesic, *Green Chem.* 12 (2010) 1493–1513.
- [4] F.W. Lichtenthaler, *Carbohydr. Res.* 313 (1998) 69–89.
- [5] M.J. Climent, A. Corma, S. Iborra, *Green Chem.* 13 (2011) 520–540.
- [6] K.J. Zeitsch, *The Chemistry and Technology of Furfural and its Many By-Products*, Elsevier Science, Amsterdam, 2000.
- [7] C. Moreau, R. Durand, D. Peyron, J. Duhamet, P. Rivalier, *Ind. Crops Prod.* 7 (1998) 95–99.
- [8] S. Lima, M. Pillinger, A.A. Valente, *Catal. Commun.* 9 (2008) 2144–2148.
- [9] R. O'Neill, M.N. Ahmad, L. Vanoye, F. Aiouache, *Ind. Eng. Chem. Res.* 48 (2009) 4300–4306.
- [10] S. Lima, M.M. Antunes, A. Fernandes, M. Pillinger, M.F. Ribeiro, A.A. Valente, *Appl. Catal., A* 388 (2010) 141–148.
- [11] S.B. Kim, S.J. You, Y.T. Kim, S. Lee, H. Lee, K. Park, E.D. Park, *Korean J. Chem. Eng.* 28 (2011) 710–716.
- [12] A.S. Dias, S. Lima, M. Pillinger, A.A. Valente, *Catal. Lett.* 114 (2007) 151–160.
- [13] X. Shi, Y. Wu, P. Li, H. Yi, M. Yang, G. Wang, *Carbohydr. Res.* 346 (2011) 480–487.
- [14] S. Lima, A. Fernandes, M.M. Antunes, M. Pillinger, F. Ribeiro, A.A. Valente, *Catal. Lett.* 135 (2010) 41–47.
- [15] A.S. Dias, S. Lima, D. Carriazo, V. Rives, M. Pillinger, A.A. Valente, *J. Catal.* 244 (2006) 230–237.
- [16] A.S. Dias, S. Lima, M. Pillinger, A.A. Valente, *Carbohydr. Res.* 341 (2006) 2946–2953.
- [17] A.S. Dias, M. Pillinger, A.A. Valente, *Appl. Catal., A* 285 (2005) 126–131.
- [18] A.S. Dias, M. Pillinger, A.A. Valente, *J. Catal.* 229 (2005) 414–423.
- [19] X. Shi, Y. Wu, H. Yi, G. Rui, P. Li, M. Yang, G. Wang, *Energies* 4 (2011) 669–684.
- [20] G.H. Jeong, E.G. Kim, S.B. Kim, E.D. Park, S.W. Kim, *Microporous Mesoporous Mater.* 144 (2011) 134–139.

- [21] I. Agirrezabal-Telleria, J. Requies, M.B. Güemez, P.L. Arias, *Appl. Catal., B* 115–116 (2012) 169–178.
- [22] I. Agirrezabal-Telleria, A. Larreategui, J. Requies, M.B. Gómez, P.L. Arias, *Bioresour. Technol.* 102 (2011) 7478–7485.
- [23] V. Heguaburu, J. Franco, L. Reina, C. Tabárez, G. Moyna, P. Moyna, *Catal. Commun.* 27 (2012) 88–91.
- [24] A. Takagaki, M. Ohara, S. Nishimura, K. Ebitani, *Chem. Lett.* 39 (2010) 838–840.
- [25] A. Chareonlimkun, V. Champreda, A. Shotipruk, N. Laosiripojana, *Bioresour. Technol.* 101 (2010) 4179–4186.
- [26] I. Agirrezabal-Telleria, F. Hemmann, C. Jäger, P.L. Arias, E. Kemnitz, *J. Catal.* 305 (2013) 81–91.
- [27] C. Carlini, M. Giuttari, A.M. Raspolli Galletti, G. Sbrana, T. Armadori, G. Busca, *Appl. Catal., A* 183 (1999) 295–302.
- [28] P. Carniti, A. Gervasini, S. Biella, A. Auroux, *Catal. Today* 118 (2006) 373–378.
- [29] F. Yang, Q. Liu, X. Bai, Y. Du, *Bioresour. Technol.* 102 (2011) 3424–3429.
- [30] K. Nakajima, Y. Baba, R. Noma, M. Kitano, J.N. Kondo, S. Hayashi, M. Hara, *J. Am. Chem. Soc.* 133 (2011) 4224–4227.
- [31] J.M. Jehng, I.E. Wachs, *J. Mol. Catal.* 67 (1991) 369–387.
- [32] J. Datka, A.M. Turek, J.M. Jehng, I.E. Wachs, *J. Catal.* 135 (1992) 186–199.
- [33] F.M.T. Mendes, C.A. Perez, R.R. Soares, F.B. Noronha, M. Schmal, *Catal. Today* 78 (2003) 449–458.
- [34] V.S. Braga, J.A. Dias, S.C.L. Dias, J.L. de Macedo, *Chem. Mater.* 17 (2005) 690–695.
- [35] A.S. Dias, S. Lima, P. Brandão, M. Pillinger, J. Rocha, A.A. Valente, *Catal. Lett.* 108 (2006) 179–186.
- [36] C. García-Sancho, I. Sádaba, R. Moreno-Tost, J. Mérida-Robles, J. Santamaría-González, M. López-Granados, P. Maireles-Torres, *ChemSusChem* 6 (2013) 635–642.
- [37] I. Sádaba, S.B. Lima, A.A. Valente, M. López Granados, *Carbohydr. Res.* 346 (2011) 2785–2791.
- [38] H. Amiri, K. Karimi, S. Roodpeyma, *Carbohydr. Res.* 345 (2010) 2133–2138.
- [39] R. Weingarten, J. Cho, W.C. Conner Jr., G.W. Huber, *Green Chem.* 12 (2010) 1423–1429.
- [40] J. Zhanga, J. Zhuanga, L. Lina, S. Liub, Z. Zhanga, *Biomass Bioenergy* 39 (2012) 73–77.
- [41] J.N. Chheda, Y. Román-Leshkov, J.A. Dumesic, *Green Chem.* 9 (2007) 342–350.
- [42] M.J. Campos-Molina, R. Mariscal, M. Ojeda, M. López-Granados, *Bioresour. Technol.* 126 (2012) 321–327.
- [43] T. Sako, T. Sugeta, N. Nakazawa, T. Okubo, M. Sako, *J. Chem. Eng. Jpn.* 25 (1992) 372–377.
- [44] W. Sangarunlert, P. Piumsomboon, S. Ngamprasertsith, *Korean J. Chem. Eng.* 24 (2007) 936–941.
- [45] Y.C. Kim, H.S. Lee, *J. Ind. Eng. Chem.* 7 (2001) 424–429.
- [46] I. Agirrezabal-Telleria, J. Requies, M.B. Güemez, P.L. Arias, *Green Chem.* 14 (2012) 3132–3140.
- [47] I. Agirrezabal-Telleria, C. García Sancho, P. Maireles Torres, P.L. Arias, *Chin. J. Catal.* 34 (2013) 1402–1406.
- [48] A. Infantes-Molina, J. Mérida-Robles, P. Braos-García, E. Rodríguez-Castellón, E. Finocchio, G. Busca, P. Maireles-Torres, A. Jiménez-López, *J. Catal.* 225 (2004) 479–488.
- [49] M. Gómez-Cazalilla, J.M. Mérida-Robles, A. Gurbani, E. Rodríguez-Castellón, A. Jiménez-López, *J. Solid State Chem.* 180 (2007) 1130–1140.
- [50] J. Li, Y. Xu, D. Wu, Y. Sun, *Catal. Today* 148 (2009) 148–152.
- [51] N.R. Shiju, D.R. Brown, K. Wilson, G. Rothenberg, *Top. Catal.* 53 (2010) 1217–1223.
- [52] X. Gao, I.E. Wachs, M.S. Wong, J.Y. Ying, *J. Catal.* 203 (2001) 18–24.
- [53] P. Berteau, B. Delmon, *Catal. Today* 5 (1989) 121–137.
- [54] M.A. Abdel-Rehim, A.C.B. Dos Santos, V.L.L. Camorim, A. Da Costa Faro Jr., *Appl. Catal., A* 305 (2006) 211–218.
- [55] R. Weingarten, G.A. Tompsett, W.C. Conner Jr., G.W. Huber, *J. Catal.* 279 (2011) 174–182.